**Electronic Supplementary Information (ESI)**

# Tuning water oxidation reactivity by employing surfactant directed synthesis of porous $Co_3O_4$ nanomaterials

Priyajit Jash, Aravind V and Amit Paul*

Department of Chemistry
Indian Institute of Science Education and Research (IISER) Bhopal, MP 462066 (India)
Email: apaul@iiserb.ac.in

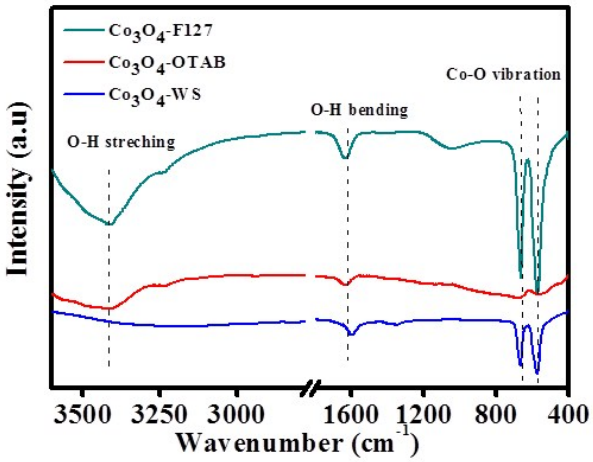


**Figure S1:** FTIR spectra of $Co_3O_4$ nanomaterials.

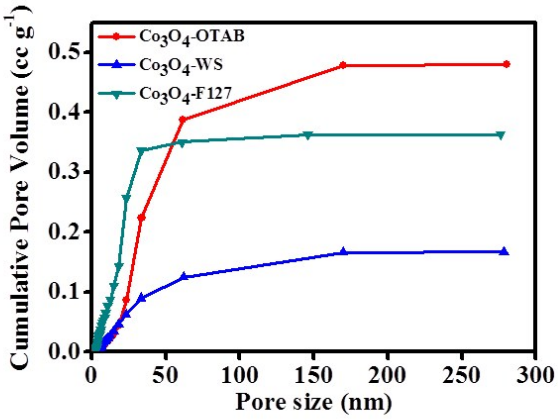


**Figure S2:** Cumulative pore volume *versus* pore size of $Co_3O_4$ nanomaterials.

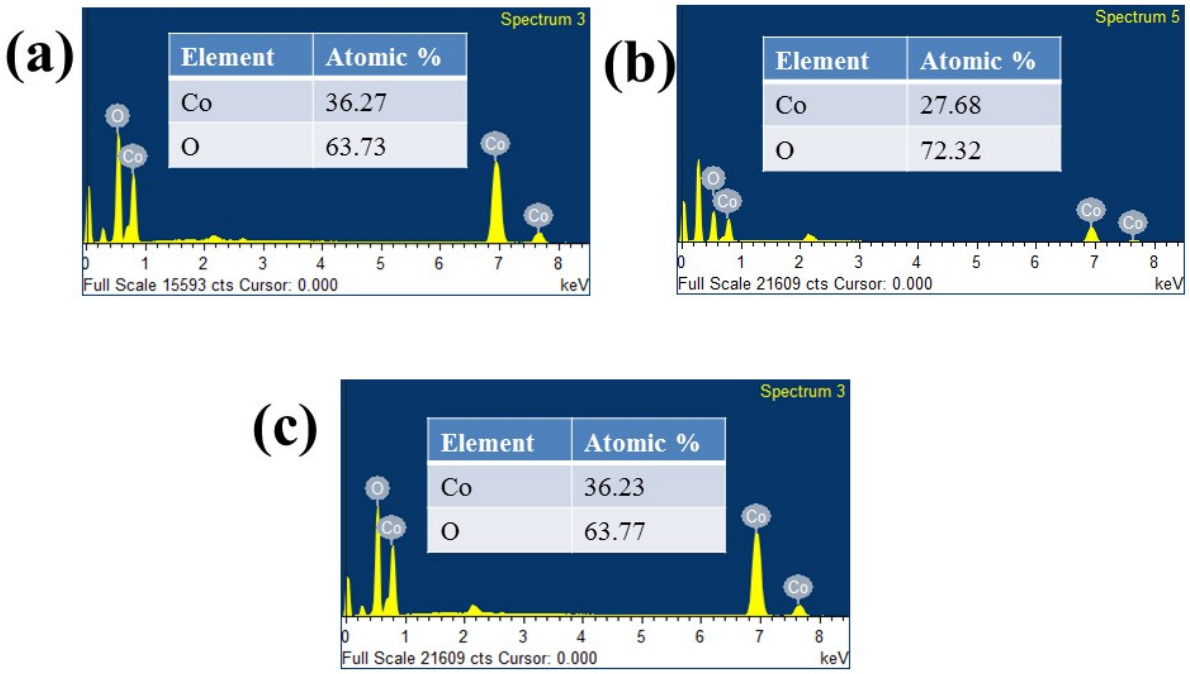


**Figure S3:** EDS mapping of (a) **$Co_3O_4$-F127** (b) **$Co_3O_4$-OTAB** and (c) **$Co_3O_4$-WS**. Inset tables show the estimated atomic weight per cent of the composition. EDS analyses were performed on carbon coated Cu grid.

**Table S1:** Literature reports of recently studied cobalt oxide based water oxidation electrocatalysts.

| Catalyst | Overpotential (η) (mV) @ 10 mA/ $cm^2$ | TOF ($s^{-1}$) | Tafel Slope (mV $dec^{-1}$) | Mass activity @η=350 (j/m; A/g) | pH | Reference |
|---|---|---|---|---|---|---|
| ***Mesoporous $Co_3O_4$ nanosheet*** | ***360*** | ***$2.86\times 10^{-1}$ @350 mV*** | ***90*** | ***123.1*** | ***14*** | ***This work*** |
| Hollow $Co_3O_4$ | 400 | $2.6 \times 10^{-3}$ @400 mV | 70 | - | 13 | *Nanoscale* 2014, **6**, 7255 |
| $Co_3O_4$ nanoparticle (~ 6 nm) | 328 | $1.87\times 10^{-2}$ @328 mV | 47±7 | - | 14 | *J. Phys. Chem. C* 2009, **113**, 15068 |
| Mesoporous $Co_3O_4$ | 476 | $4.55 \times 10^{-3}$ @400 mV | 53 | - | 13 | *Nano Res.* 2013, **6**, 47 |
| Mesoporous $Co_3O_4$ | 427 | - | - | - | 14 | *Chem. Mater.* 2013, **25**, 4926 |
| Mesoporous $Co_3O_4$ nanoflakes | 380 | - | 48 | - | 14 | *ACS Appl. Mater. Interfaces* 2015, **7**, 3306 |
| Porous $Co_3O_4$ nanoplates | 523 | $2.81\times 10^{-3}$ @400 mV | 71 | - | 14 | *J. Mater. Chem. A* 2015, **3**, 8107 |
| $Co_3O_4$ nanorods/MCNT | 309 | $5.3\times 10^{-2}$ @300 mV | 51 | - | 14 | *J. Mater. Chem. A* 2015, **3**, 1761 |
| $ZnCo_2O_4$/N-CNT | 420 | - | 70.6 | - | 14 | *Adv. Mater.* 2016, **28**, 3777 |
| $ZnCo_2O_4$/Au/CNT | 440 | 11.86 @500 mV | 46.2 | - | 14 | *J. Power Sources* 2017, **357**,1 |
| $NiCo_2P_x$/CNT | 284 | *$5.5\times 10^{-1}$* @300 mV | 50.3 | - | 14 | *J. Mater. Chem. A* 2018, **6**, 7420 |
| $NiCo_2S_4$ nanorod | 220@30 mA/ $cm^2$ | - | 113.8 | - | 14 | *J. Power Sources* 2018, **402**,116 |
| S,N-CNT/ $CoS_2$@Co | 340 | - | 76.1 | - | 14 | *Science Bull.* 2018, **63**, 1130 |
| CoOOH nanosheets | 300 | $9\times 10^{-2}$ @300 mV | 38 | 66.6 @300 mV | 14 | *Angew. Chem., Int. Ed.* 2015, **54,** 8722 |
| CoMn LDH nanosheets | 324 | $0.9\times 10^{-2}$ @300 mV | 43 | 18.8 @300 mV | 14 | *J. Am. Chem. Soc*. 2014, **136,** 16481 |

| | | | | | | |
|---|---|---|---|---|---|---|
| CoCo LDH nanosheets | 353 | $3\times 10^{-3}$ @300 mV | 45 | - | 14 | *Nat. Commun.* 2014, **5**, 4477 |
| FeCoMo | 460 | $5.89\times 10^{-2}$@350 mV | 29 | 46.8 | 14 | *New J. Chem.* 2018, **42**, 7254 |
| α $Co(OH)_2$ nanomesh | 303 | - | 69 | 31.3@303 mV | 14 | *Chem. Commun.* 2018, **54,** 4045 |
| α $Co(OH)_2$ nanosheet | 317 | - | 49 | 2.9@303 mV | 14 | *Chem. Commun.* 2018, **54,** 4045 |
| CoOP Hollow nanocage | 380 | $1.62\times 10^{-2}$ @350 mV | 67 | 41.7 | 14 | *Chem. Eur. J.* 2017, **23,** 12519 |

**Calculation of areal capacitance ($C_{DL}$, µF/cm$^2$), electrochemically accessible surface area (ECSA) and roughness factor (RF)**

The charging current for cathodic ($i_c$) and anodic ($i_a$) currents were taken at 0 V *versus* Ag/AgCl. The relation between $i_c/i_a$ *versus* scan rate (ν) and the double layer capacitance (C) were given by equations S1 (a-b).

$$i_a = \nu C \quad \text{..... (S1a)}$$

$$i_c = \nu C \quad \text{..... (S1b)}$$

The slopes of $i_c$ and $i_a$ as a function of ν provided C from the slope. The average slope calculated from cathodic and anodic currents was taken as C. The geometrical area of the electrode (GSA) was 0.07 cm$^2$. The areal capacitances ($C_{dl}$, µF/cm$^2$) were calculated by dividing C with GSA

For the calculation of electrochemically accessible surface area (ECSA), equation S2 has been used wherein $C_s$=27 µF/cm$^2$ (specific surface area) taken from the literature.[1]

**ECSA** = $C/C_S$ …… (S2)

Roughness factor (RF) was estimated using equation S3.

**Roughness Factor (RF)** = ECSA/GSA ……. (S3)

**Table S2:** Non-faradic capacitances ($C_{dl}$), electrochemically accessible surface areas (ECSA), and roughness factors (RF) of $Co_3O_4$ nanomaterials.

| Sample | Capacitance $C_{dl}$ (µFcm$^{-2}$) | ECSA (cm$^2$) | Roughness Factor (RF) |
|---|---|---|---|
| **$Co_3O_4$-F127** | 42.8 | 1.58 | 22.6 |
| **$Co_3O_4$-OTAB** | 19.3 | 0.71 | 10.1 |
| **$Co_3O_4$-WS** | 8.80 | 0.32 | 4.6 |

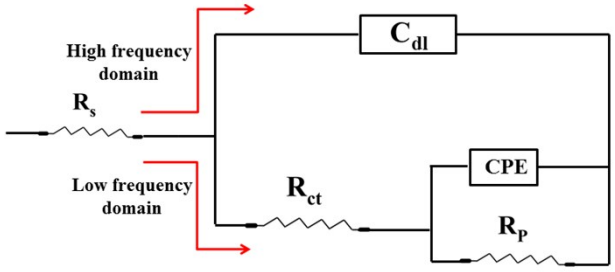


**Figure S4:** Equivalent circuit model used for fitting of OER catalysis results by $Co_3O_4$ nanomaterials. $R_s$, $C_{dl}$, $R_{ct}$, $R_p$, and CPE represent uncompensated solution resistance, double layer charging at the electrode/electrolyte interface at high frequency domain, charge transfer resistance at the electrode/electrolyte interface related to the overall OER, pseudoresistance

which is related with one or more surface intermediates formation, and pseudocapacitance which represents change in charged surface species as OER proceeds respectively.

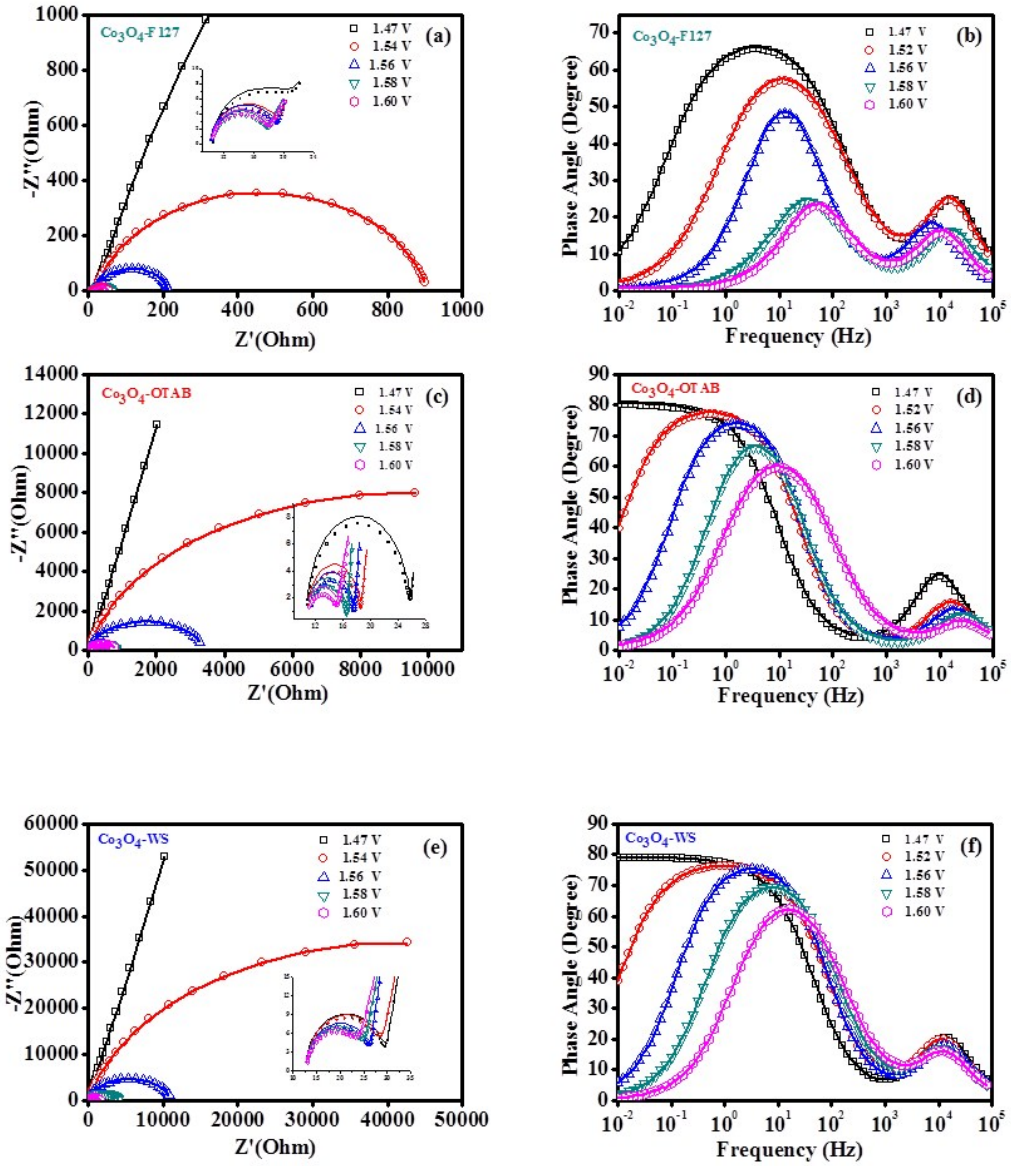


**Figure S5:** Potential dependent EIS results for OER by $Co_3O_4$ nanomaterials. Nyquist plots for (a) **$Co_3O_4$-F127** (c) **$Co_3O_4$-OTAB** and (e) **$Co_3O_4$-WS** respectively (inset shows the high frequency region). Bode plots for (b) **$Co_3O_4$-F127** (d) **$Co_3O_4$-OTAB** and (f) **$Co_3O_4$-WS**. The experimental results were represented by discrete points, while simulated impedance results were represented by continues lines.

**Table S3:** Equivalent circuit parameters calculated from EIS fitting for $Co_3O_4$ nanomaterials at different potentials.

| | $Co_3O_4$-WS | | | | | | $Co_3O_4$-OTAB | | | | | |
|---|---|---|---|---|---|---|---|---|---|---|---|---|
| E/V (*vs.* RHE) | $R_S$ (Ω) | $\mathbf{R_{Ct}}$ **(Ω)** | $C_{dl}$ (μ F) | $\mathbf{R_P}$ **(Ω)** | $Q$ ($Fs^{(a-1)}$) | Exp (a) | $R_S$ (Ω) | $\mathbf{R_{Ct}}$ **(Ω)** | $C_{dl}$ (μ F) | $\mathbf{R_P}$ **(Ω)** | $Q$ ($Fs^{(a-1)}$) | Exp (a) |
| 1.47 | 15.9 | 17 | 0.9 | 0 | 0.00021 | 0.87 | 11.0 | 15 | 1.7 | 0 | 0.0010 | 0.89 |
| 1.52 | 15.9 | 15 | 1.1 | 84100 | 0.00012 | 0.87 | 10.8 | 9.2 | 1.6 | 18800 | 0.00061 | 0.89 |
| 1.56 | 15.8 | 13 | 1.2 | 11000 | 0.00011 | 0.90 | 10.9 | 9 | 1.6 | 3389 | 0.00050 | 0.90 |
| 1.58 | 15.9 | 11 | 1.3 | 4307 | 0.00010 | 0.87 | 11.1 | 7.5 | 1.3 | 821.4 | 0.00049 | 0.91 |
| 1.60 | 15.8 | 10 | 1.3 | 1564 | 0.00010 | 0.84 | 11.0 | 6.8 | 1.6 | 799.8 | 0.00029 | 0.82 |

| | $Co_3O_4$-F127 | | | | | |
|---|---|---|---|---|---|---|
| E/V (*vs.* RHE) | $R_S$ (Ω) | $\mathbf{R_{Ct}}$ **(Ω)** | $C_{dl}$ (μ F) | $\mathbf{R_P}$ **(Ω)** | $Q$ ($Fs^{(a-1)}$) | Exp (a) |
| 1.47 | 13 | 13.7 | 0.7 | 14300 | 0.00012 | 0.86 |
| 1.52 | 10.5 | 7.4 | 0.8 | 2162 | 0.00014 | 0.85 |
| 1.56 | 10.3 | 6.2 | 4.2 | 195.3 | 0.00037 | 0.84 |
| 1.58 | 10.3 | 5.2 | 3.3 | 43.6 | 0.00043 | 0.84 |
| 1.60 | 10.5 | 3.8 | 2.4 | 42 | 0.00059 | 0.79 |

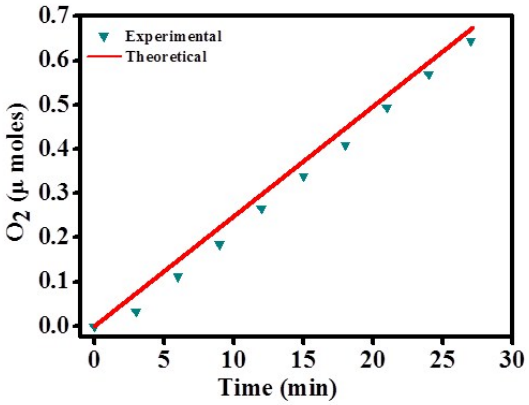


**Figure S6:** Theoretical (red line) and experimental (dark cyan triangle) quantification of $O_2$ evolution with **$Co_3O_4$-F127** catalyst at 1.62 V (*vs.* RHE) in 1 M NaOH during chronoamperometrty

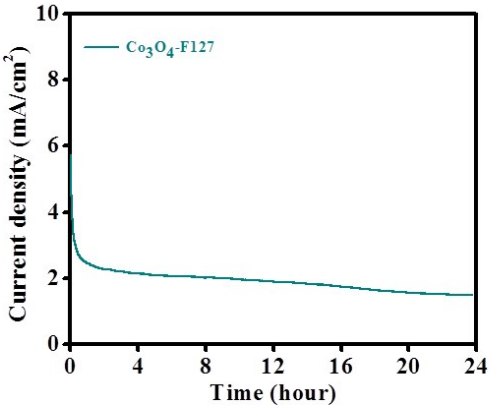


**Figure S7:** Chronoamperogram showing the stability up to 24 h at a constant potential of 1.58 V (*vs.* RHE) in 1 M NaOH during water oxidation

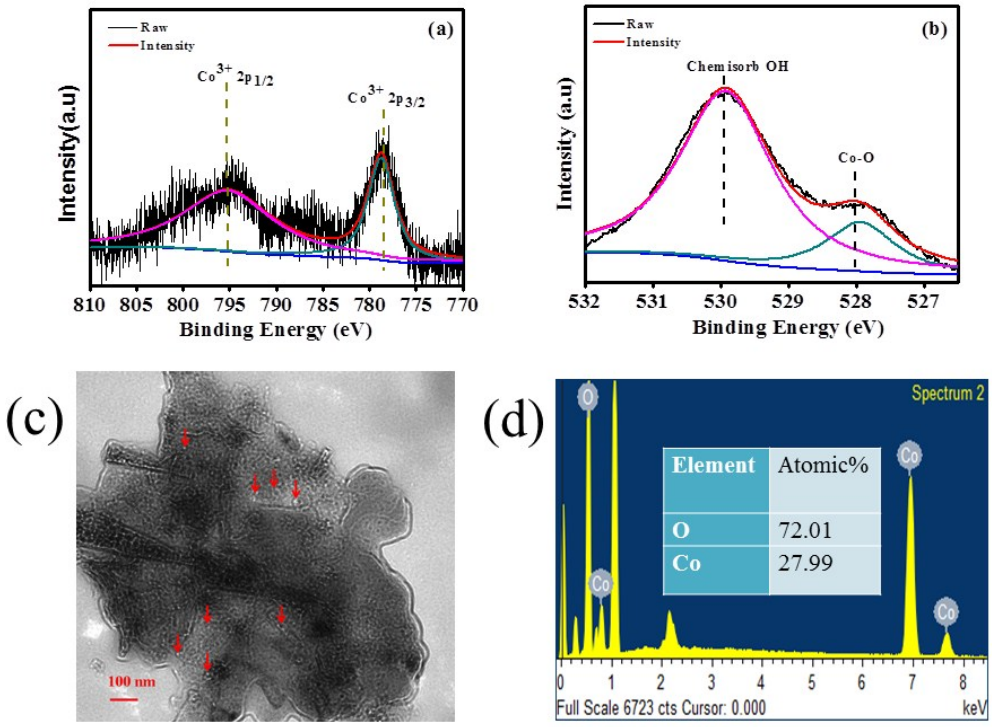


**Figure S8:** (a) & (b) XPS spectra of Co and O respectively of **$Co_3O_4$-F127** after long term chronoamperometry experiment on ITO glass substrate at 1.58 V (*versus* RHE) in 1 M NaOH solution. (c) TEM image of **$Co_3O_4$-F127** after long term chronoamperometry experiment on ITO coated glass substrate at 1.58 V (*versus* RHE) in 1 M NaOH solution (pores shown by red arrows). (d) Corresponding EDS analysis.

**References:**

1. C. C. L. McCrory, S. H. Jung, J. C. Peters and T. F. Jaramillo, *J. Am. Chem. Soc.*, 2013, **135**, 16977-16987.